

## Electron Temperature and Density Inferred from JET ECE Diagnostics

S. Schmuck<sup>1</sup>, J. Svensson<sup>2</sup>, L. Figini<sup>3</sup>, T. Jonsson<sup>4</sup>, J. Fessey<sup>1</sup>, L. Meneses<sup>5</sup>, J.E. Boom<sup>6</sup> and  
JET EFDA Contributors\*

JET-EFDA, Culham Science Centre, Abingdon, OX14 3DB, UK

<sup>1</sup>*CCFE, Culham Science Centre, Abingdon, Oxon, OX14 3DB, UK*

<sup>2</sup>*Max-Planck-Institut für Plasmaphysik, Teilinstitut Greifswald, EURATOM-Assoziation, D-17491 Greifswald, Germany*

<sup>3</sup>*Istituto di Fisica del Plasma, CNR, Euratom-ENEA-CNR Association, Milano, Italy*

<sup>4</sup>*Fusion Plasma Physics, EES, KTH, SE-10044 Stockholm, Sweden*

<sup>5</sup>*Instituto de Plasmas e Fusão Nuclear, Instituto Superior Técnico, Universidade de Lisboa, 1049-001 Lisboa, Portugal*

<sup>6</sup>*Max-Planck-Institut für Plasmaphysik, Boltzmannstraße 2, D-85748 Garching, Germany*

### 1. Introduction

At JET the electron cyclotron emission (ECE) spectrum of several harmonics (up to 500 GHz) mainly in X-mode polarisation is probed by a Michelson interferometer [1,2] and a heterodyne radiometer [3]. For a wide range of plasma parameters the optical thickness of the medium for the spectral range 100 GHz - 200 GHz is assumed to be suited to justify the black-body approach used as a standard at JET. This links the radiative temperature associated with the measured ECE spectrum in the domain of the second harmonic with the electron temperature profile. However, from theoretical point of view the full ECE spectrum provides additional information: about the electron density, and also about the equilibrium. To exploit this information the ECE ray-tracing code SPECE [4,5] and TRAVIS [6] have been used to model the measured ECE spectrum dependent on the profiles and equilibrium. Due to the embedding of the ray-tracing code SPECE into the Bayesian framework Minerva [7] a powerful tool is available to infer the density and temperature profile relying only on the ECE diagnostic model. A proof of principle was demonstrated [8]. With this approach, corrected temperature profiles not relying on the assumption of optical thickness, can be inferred, and compared to the results derived from the standard approach. It will also be shown how much information about the electron density profiles can be derived from the measured spectra. Besides those profiles, a correction of the vacuum magnetic field and the wall reflection properties are considered as free parameters in the probabilistic approach presented.

### 2. Predictive Model for ECE Spectrum

The ECE spectrum  $T_{RAD}^{SIM}$  in terms of radiative temperature is predicted by the ray-tracing code SPECE based on the physics of the involved waves in the plasma medium. Basically, for given input quantities SPECE evaluates the refractive index, absorption and emission along the ray trajectories to

---

\* See the Appendix of F. Romanelli et al., Proceedings of the 24th IAEA Fusion Energy Conference 2012, San Diego, US

solve the radiation transport equation. Thereby, the dispersion relation and the dielectric tensor in fully relativistic notion enter. The main input quantities are the frequencies at which the spectrum should be evaluated, vacuum line of sight of the diagnostic, poloidal flux map, poloidal current function, wall reflection coefficient ( $W_R$ ) enhancing the radiation and mode scrambling coefficient ( $W_{MS}$ ) mixing X- and O-mode polarised radiation at each reflection on the wall, the electron density ( $n_e$ ) and temperature ( $T_e$ ) profiles. Furthermore, the vacuum magnetic field ( $B_0$ ) may be scaled.

### 3. Minerva

The predictive model is embedded in the Bayesian inference framework Minerva to achieve the inference of the free parameters  $T_e$ ,  $n_e$ ,  $B_0$ ,  $W_R$  and  $W_{MS}$  by a probabilistic approach. The framework optimises the posterior distribution with respect to the free parameters. The inverse of the Hessian matrix, being the second order partial derivatives of the negative logarithm of the posterior at the found maximum, estimates the variance-covariance matrix for the inferred quantities. The temperature and density profiles are parameterised each by a number of values located in the normalised poloidal flux range  $[0,1]$  and are forced to vanish at  $\psi_N=1.05$ . For each profile the associated prior is chosen to be a multivariate normal distribution with vanishing mean and a covariance matrix derived from a squared exponential Gaussian process. Thereby, the prior has large entries along the main diagonal, and off-diagonal elements are chosen such that the scale length, for which changes occur, is  $\Delta\psi_N=0.2$ . Uniformly distributed priors,  $B_0$  in  $[0.95* B_{0EFIT}, 1.05* B_{0EFIT}]$ ,  $W_R$  and  $W_{MS}$  in  $[0,1]$ , limit these parameters to reasonable domains. The likelihood itself is a multivariate normal connecting the prediction with the data. The uncertainty on the data is set to  $\sigma_D = 0.05$  keV exceeding the statistical uncertainties of the diagnostic calibration by a factor  $\sim 2$ .

### 4. Inference

The inference is performed at the time 7.21 s for the JET pulse 85776 (L-mode discharge,  $B_{0EFIT}=3.4$  T,  $I_{PLA}=2.2$  MA,  $P_{NBI}=2.3$  MW,  $n_e dl=5.5 \times 10^{19} \text{m}^{-2}$ ). The poloidal flux and current function are taken from standard EFIT output. Only the central ray of the line of sight is used.

The inference is split into two steps, since the wall properties are unknown for the ITER-Like Wall (ILW) so far. In the first step the density profile JET is held constant provided by the reflectometer and assumed to be accurate and precise (see Fig. 1a). The inference is made only on the  $T_e$  profile represented by 23 values,  $B_0$ ,  $W_R$  and  $W_{MS}$ . Those inferred quantities are kept constant in the second step to estimate the  $n_e$  profile represented by 23 free parameters. Step 1: Since checks show that the initial guess for  $T_e$  does not affect the outcome, the temperature profile determined by the standard approach for the Michelson itself is taken (see Fig. 1a). Note, for the standard approach  $T_e$  is not constant on a given flux surface per se. As initial values  $B_0 = 3.4$  T and  $W_R = W_{MS} = 0$  (single-pass through the plasma) are set. In total, 26 parameters are to be inferred.

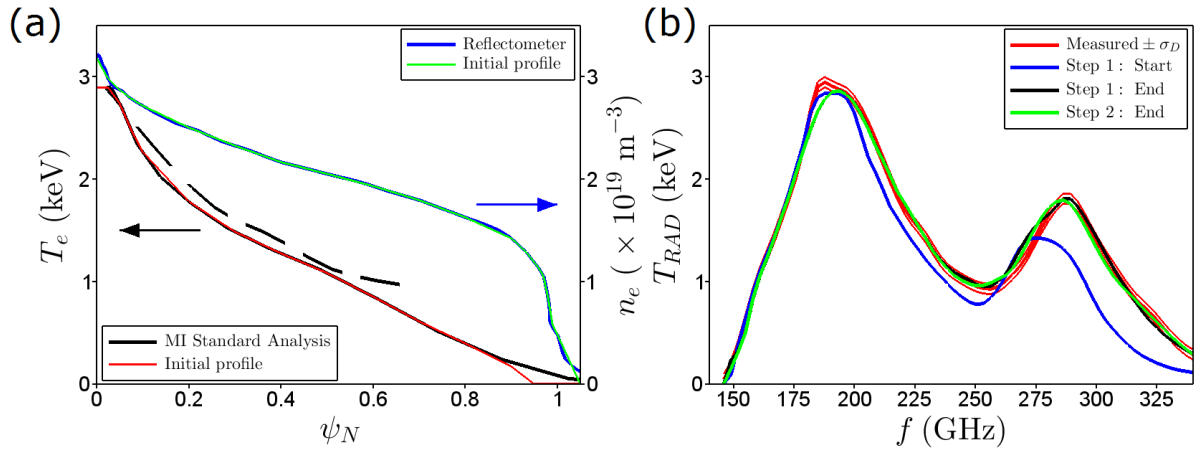


Fig. 1. (a)  $T_e$  profile (black) determined by standard approach (not preserved on flux surface) and  $n_e$  profile (blue) determined by reflectometer for JET pulse 85776,  $t=7.21$  s. The initial guess for  $T_e$  (red) is used in the first step keeping  $n_e$  (green) constant. (b) ECE spectra measured by Michelson and evaluated by SPECE for different parameter sets.

The ECE spectra  $T_{RAD}$  and  $T_{RAD}^{SIM}$  corresponding to the start and end of the optimisation are shown in Fig. 1b for the spectral range 146 GHz – 340 GHz (2<sup>nd</sup> and 3<sup>rd</sup> harmonic) with increment  $\Delta f = 3$  GHz. The final  $T_{RAD}^{SIM}$  agrees with the data within the uncertainties. However, systematic deviations are present close to the peak of the second harmonic range and for the spectral range 260 GHz – 290 GHz. Both ranges are strongly linked with the plasma centre. The estimated  $T_e$  profile is increased for  $\psi_N < 0.7$  by roughly 0.15 keV with respect to the results from the standard approach (see Fig. 2a). For  $0.9 < \psi_N < 1.0$  the temperature remains finite at about 0.3 keV. The uncertainties  $\sigma_{T_e}$  are estimated to be 0.03 keV in the plasma centre, 0.12 keV at  $\psi_N=0.8$  and 0.01 keV nearby  $\psi_N=1$ . Regarding the vacuum magnetic field, the estimation gives an increase to  $\sim 3.45$  T (1.44%) with  $\sigma_{B_0} = 0.001$  T. For  $W_R$  and  $W_{MS}$  the determined values read  $\sim 0.6$  and 0.16 having  $\sigma_{W_R} = 0.06$  and  $\sigma_{W_{MS}} = 0.15$ , respectively. Furthermore, these coefficients have a high correlation ( $\rho=0.97$ ). Step 2: As initial guess for  $n_e$  one tenth of the density profile measured by the reflectometer is set (see Fig. 1a). The result disagrees with the reflectometer density systematically (see Fig. 2b). Nevertheless, the shape resembles the reference one in lowest order, and the central values are similar. The uncertainties are about  $0.05 \times 10^{19} \text{ m}^{-3}$ .

## 5. Discussion/Conclusion

The probabilistic, i.e., Bayesian approach presented enables the inference on the  $T_e$  and  $n_e$  profiles, the magnetic field correction and wall properties. Thereby, contrary to the standard approach, the underlying physics captured by the ECE ray-tracing code SPECE is exploited. Furthermore, the constancy of  $T_e$  and  $n_e$  on a flux surface is guaranteed. The inferred  $T_e$  profile turns out to be reasonable apart from the plasma edge when compared to the ones gained by the standard approach and the high resolution Thomson scattering diagnostic (see Fig. 2a). The  $n_e$  profile disagrees systematically from reflectometer results (see Fig. 2b). The determined increase of the vacuum magnetic field by 1.44% is

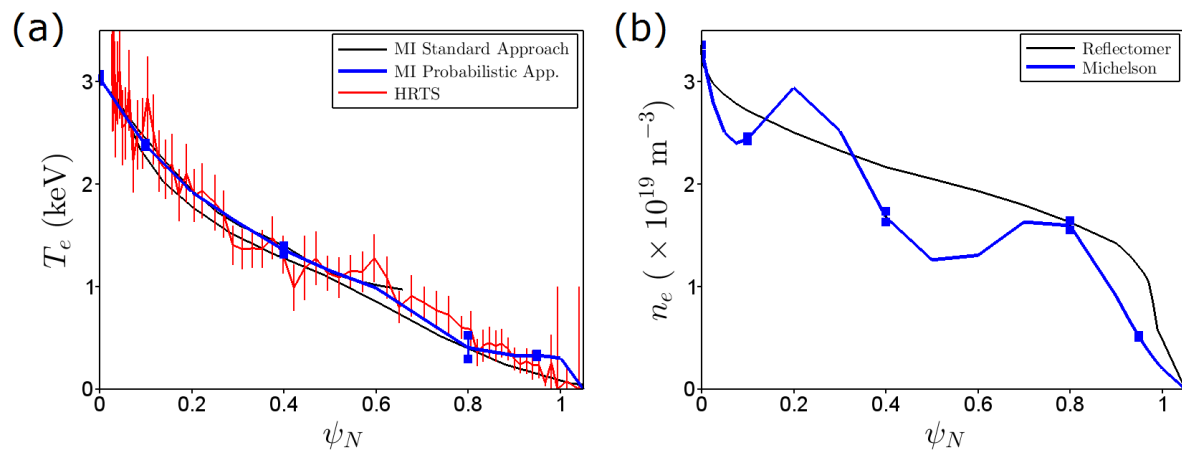


Fig. 2. (a)  $T_e$  profiles determined by different approaches for Michelson and high resolution Thomson scattering diagnostic (HRTS). The uncertainties estimated by probabilistic approach: 0.034 keV, 0.017 keV, 0.042 keV, 0.115 keV and 0.013 keV with increasing  $\psi_N$ . (b)  $n_e$  profiles determined by reflectometer and probabilistic approach for Michelson. The uncertainties are below  $0.05 \times 10^{19} \text{ m}^{-3}$ .

a typical value which other diagnostics, like the reflectometer, apply to achieve inter-diagnostic consistency by profile shifting. In addition, the finding is close to the increase of 1.6% determined by the recent upgrade in measuring the toroidal field coil current at JET[9]. While the reflectivity of the JET-ILW found here is in the very vicinity of the value 0.55 estimated by manual analysis using SPECE for the JET Carbon wall[10], the mode scrambling coefficient ( $\sim 0.16$ ) estimated differs considerably from 0.35 in [10]. Improvements in the determination for the  $T_e$  profile are expected, especially at the plasma edge, once the heterodyne radiometer with higher spectral resolution is incorporated in the probabilistic approach. Since, virtually, no other constraint on the density was used here, the inference of the density might be improved by additional constraints like the limitation to negative gradients only. Furthermore, the model for the line-integrated density diagnostic at JET already existent in Minerva could be connected to ECE diagnostic model. The derived uncertainties, at least for the profiles, are very small. Further studies need to be done in that matter.

### Acknowledgment

This project has received funding from the European Union's Horizon 2020 research and innovation programme under grant agreement number 633053 and from the RCUK Energy Programme [grant number EP/I501045]. The views and opinions expressed herein do not necessarily reflect those of the European Commission.

### References

- [1] A. E. Costley et al., Proceedings of EC-3 Conference (1982)
- [3] E. de la Luna, J. Sánchez, V. Tribaldos, et al., Rev. Sci. Instrum. 75, 3831 (2004)
- [4] D. Farina, L. Figini, P. Platania, and C. Sozzi, AIP Conf. Proc. 988, 128 (2008)
- [5] L. Figini et al., Rev. Sci. Instrum. 81, 10D937 (2010)
- [6] N.B. Marushchenko, Y. Turkin, H. Maassberg, Computer Physics Comm. 185 (2014)
- [7] J. Svensson and A. Werner, Proc. IEEE WISP (2007)
- [8] S. Schmuck et al., Proceedings of 38<sup>th</sup> EPS Conference (2011)
- [9] Eva Belonohy, et al, Abstract send to 28th SOFT (2014)
- [10] L. Barrera, et al, Plasma Phys. Control. Fusion 52, 085010 (2010)